Analytical modelling and validation of the expansion of a CO 2 jet released from a ruptured pipeline

4 authors:

Wentian Zheng
University College London
10 PUBLICATIONS   **15** CITATIONS

SEE PROFILE

Solomon Brown
The University of Sheffield
95 PUBLICATIONS   **939** CITATIONS

SEE PROFILE

Sergey B Martynov
University College London
79 PUBLICATIONS   **746** CITATIONS

SEE PROFILE

Haroun Mahgerefteh
University College London
125 PUBLICATIONS   **1,066** CITATIONS

SEE PROFILE

Some of the authors of this publication are also working on these related projects:

Project   Quantitative Safety Assessment of Hydrocarbon Transportation Pipelines View project

Project   COOLTRANS View project

Analytical modelling and validation of the expansion of a CO_2 jet released from a ruptured pipeline

W.Zheng[1, *], S.Brown[1], S.Martynov[1] and H.Mahgerefteh[1]

[1]*Department of Chemical Engineering, University College London, London WC1E7JE, United Kingdom, wentian.zheng.14@ucl.ac.uk*

Abstract – The transportation of pressurised CO_2 using pipelines is a crucial element of the Carbon Capture and Storage (CCS) chain; for their safe design the ability to accurately predict the consequences of a failure, the jet release and ensuing dispersion is essential. Such phenomena are commonly modelled in stages: jet expansion followed by atmospheric dispersion. For jet expansion modelling, both analytical and Computational Fluid Dynamic (CFD) models are available to predict the fully expanded flow conditions which are subsequently used as inputs in dispersion modelling. Although analytical models are computationally efficient, due to the lack of experimental data, their predictions have yet been verified. In this work, a conservation law based multiphase analytical model is constructed with a rigorous equation of state. The predicted flow variables at full expansion are then compared to those from the Shear Stress Transport k-ω CFD model. The quantitative comparisons between two models provide necessary verification of the application of analytical models in accidental release modelling.

1. Introduction

Transportation of highly pressurised CO_2 through pipeline networks is a crucial component of the Carbon Capture and Storage (CCS) technology [1, 2]. The International Energy Agency [3] has suggested that, by 2030, approximately 100,000 km of CO_2 pipelines will be built across the world. In order to keep CCS an economically viable option for carbon reduction, CO_2 pipeline routing through highly populated areas cannot be completely avoided [4]. Given that transportation by pipelines will likely be performed in dense or supercritical phase [5, 6], unplanned releases pose a significant hazard to human populations due to the potentially large volume and the fact that CO_2 is an asphyxiant. Therefore, it is of great importance to develop an accurate and industrially practical modelling strategy for such accidental releases.

At the onset of an accidental release, the expansion and acceleration of highly pressurised CO_2 from the pipe results in a supersonic jet, creating shocks and inducing phase change in the pipe, as well as close to the discharge plane. Thermodynamic process is dominant in this region (Region B in Figure 1). After the jet is fully expanded (usually a few nozzle diameters downstream of the release plane), entrainment becomes important in the dispersion region (Region C) [7, 8].

In practice, the modelling of the process above is usually divided into three constituent parts corresponding to the main regions observed (Figure 1): an isentropic expansion model to predict choked conditions (orifice conditions (subscript 1)) based on reservoir conditions or stagnation conditions (subscript 0), analytical or CFD models to predict the fully expanded flow states (subscript 2) and, finally, analytical or CFD models to simulate the subsequent dispersion.
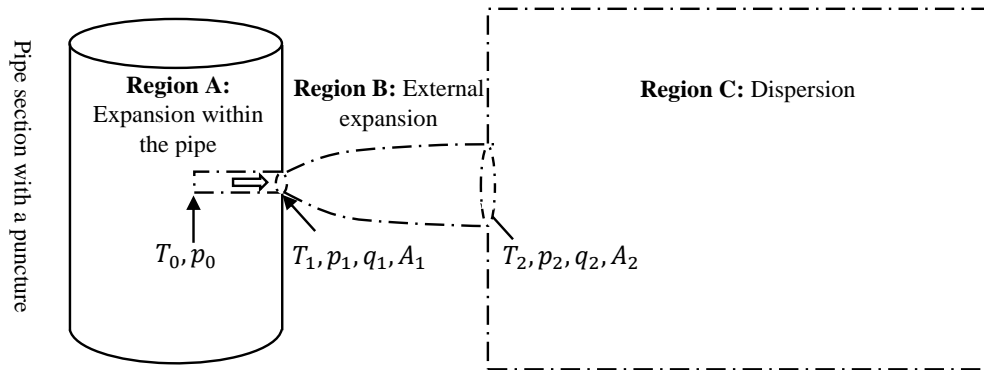
Figure 1: Schematic of three main regimes during high pressure pipeline jet releases

For Region B, although CFD models of these under-expanded jets are capable of resolving the exact flow field including phase change, turbulence interactions and discontinuities (e.g. shocks), enormous computing effort is required. X.Liu et al. [9] have conducted CFD simulations of single phase, highly under-expanded CO_2 jets, applying the standard Peng-Robinson equation of state; a computational domain of 0.49 million cells with a time step size of 1.0×10^{-7} s was reported. In the study of highly turbulent under-expanded hydrogen and methane jets by A. Hamzehloo et al. [10], it was found necessary, in order to establish the large pressure gradient close to the nozzle, to use an even smaller time step size of 5.0×10^{-9} s. Multiphase CFD simulations accounting for the solid phase formation, incorporating the modified $k\text{-}\varepsilon$ two-equation turbulence model and the dynamic adaptive meshing technique, was carried out by R.M.Woolley et al. [11], which showed that a significant level of mesh refinement at shock locations is required to accurately predict the flow field. Other studies, such as the impact of changing back pressure on shock stability by T.Irie et al. [12] and the Large Eddy Simulation of stable supersonic jets by A.Dauptain et al. [13], also reported a high computational demand to resolve discontinuities and large gradients.

As a result, analytical models are often used when details of the flow structure are not of interest. However, they are associated with a number of assumptions and simplifications; the predicted fully expanded conditions, which will be subsequently used as inputs in dispersion models, need to be verified and validated. Unfortunately, because of the sensitivity of the flow field towards fluid materials and release configurations, and the existence of rapid changes, the experimental data at such a short distance from the release plane is generally not available [7]. Therefore, the motivation of this work is to conduct CFD jet simulations with appropriate physical models to obtain the flow states at full expansion and thereby verify those predicted by analytical models.

In this work, Section 2 presents the development of the isentropic expansion model followed by descriptions of the analytical and CFD external expansion models. The general structure of the released jet is discussed in Section 3. The calculated choked conditions and fully expanded flow states by both the analytical and the CFD model are presented in Section 4 together with model comparisons and discussions. Conclusions are drawn in Section 5. The release upstream reservoir conditions are based on INERIS test 2, 3 and 4 (with pressure (p_0) at 27.0, 42.0 and 39.0bar, temperature (T_0) at 264.3, 280.1 and 278.1K) [14]. For these CO_2 release tests, the inventory is in saturated state; the releases from saturated vapour or liquid are both possible and the former scenario is analysed here. The nozzle outlet radius is 3mm.

2. Modelling approach

2.1 Multiphase modelling

The Homogeneous Equilibrium model is used throughout this work to describe multiphase behaviour during fluid expansion, in which both phases are assumed to be at the same velocity and temperature. This assumption is valid when the interphase mass transfer is fast in comparison with the time scale of the expansion.

During the expansion of CO_2 to ambient conditions, although the standard Peng-Robinson Equation of State (PR-EoS) can be applied to vapour and liquid phase, direct extension to solid phase which results from the fluid expanding below the triple point (216.6K, 5.18bar) is invalid due to the existing discontinuity at liquid-solid transition [15]. In order to model vapour/solid phase equilibrium, the Extended Peng-Robinson Equation of State (EPR-EoS), first introduced by Martynov et al., is applied in this work. Additionally, a tanh function (Eq. 1) is used to connect the liquid and solid phase saturated properties.

$$S(T) = \left(0.5 + 0.5 \times tanh\left(\frac{T - 216.6}{b}\right)\right) \tag{1}$$

$$F(T) = (1 - S(T)) \times f(T) + (S(T)) \times g(T) \tag{2}$$

Where *f(T)* and *g(T)* are functions of the liquid and solid phase saturated properties respectively, 216.6 is the numerical value of the triple point temperature for CO_2 where discontinuity occurs, and *b* is a smoothing factor. The resulted function *F(T)* ensures a continuous thermodynamic description of the condensed phase and numerical stability of the solver. Figure 2 shows the saturated thermodynamic properties of the condensed phase as a function of temperature. The discontinuity at the triple point can clearly be observed.
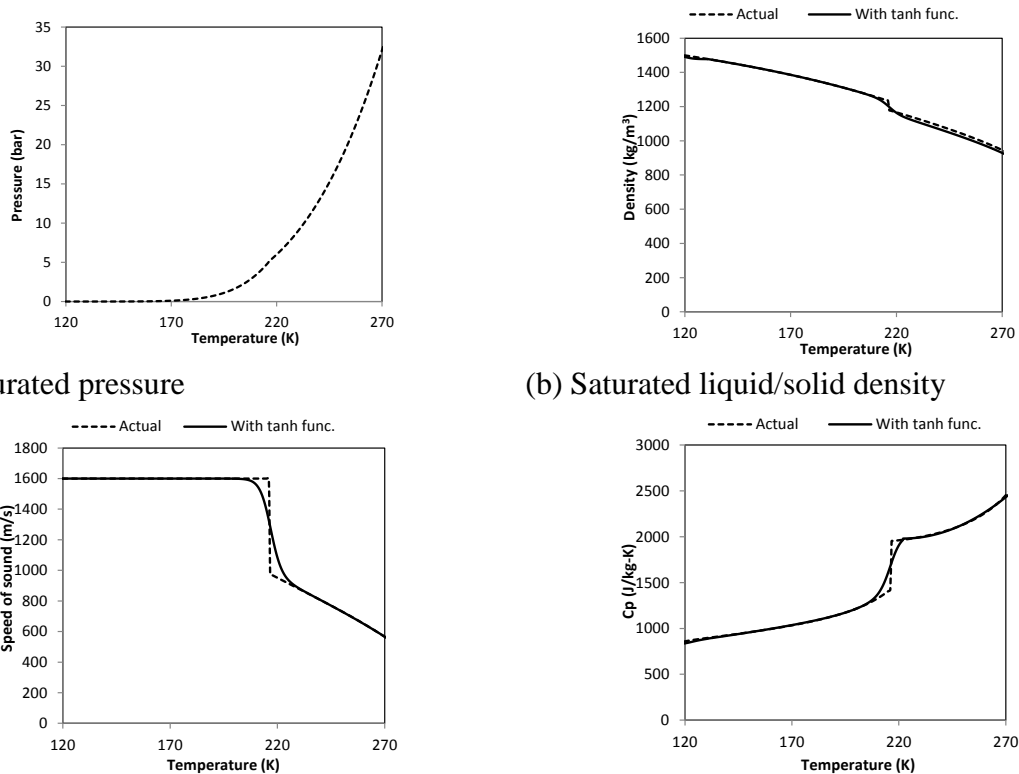
(a) Saturated pressure

(b) Saturated liquid/solid density

(c) Saturated liquid/solid speed of sound

(d) Saturated liquid/solid heat capacity

Figure 2: The saturated properties for liquid/solid phase CO_2

2.2 Predictions of choked conditions

Due to the high ratio of the pressure at release plane to ambient pressure, the flow is choked. Since the choked conditions will be used as inputs to the subsequent external expansion models, it is of great importance to give accurate predictions. Therefore, an isentropic expansion model, using the EPR-EoS described above, is applied with the additional assumptions of negligible heat transfer, reversibility and steady reservoir conditions [16]. Following an energy balance between stagnation and choked conditions, the mass flux may be written as:

$$\dot{m}_1 = \rho_1 \times \sqrt{2(h_0 - h_1)} \tag{3}$$

Where ρ_i, h_i, and $\dot{m}_i$ denote the bulk density, enthalpy and mass flux at stagnation (subscript 0) and choked conditions (subscript 1).

Since the entropy is conserved, a pressure-entropy flash is performed to determine the phase split and other thermodynamic properties (e.g. enthalpy) at different pressures. The choked conditions are then identified when the mass flux in Eq. 3 is maximised [17].

2.3 Analytical modelling of external expansion

The most commonly applied analytical models for the expansion of a jet are: the isentropic expansion model, the isenthalpic model, and the Bernoulli's equation when the fluid is in liquid phase [8, 18].

Although, the general assumption of negligible entrainment of the surrounding gas made by the models above may be valid considering the length scale of the process, each model has its own additional limitations regarding its applications. For example, the isentropic expansion model implies that there is no entropy generation during the external expansion. As will be detailed in Section 3, jet external expansion features shock formation (entropy generation), flow supersonic accelerations and significant expansions. Evidently, these three analytical models are not appropriate. Without these, but by assuming quasi-one-dimensional flow, mass, momentum and energy balances may be written:

$$\rho_1 u_1 A_1 = \rho_2 u_2 A_2 \tag{4}$$

$$-\rho_1 u_1 A_1 u_1 + \rho_2 u_2 A_2 u_2 = \int_{A1}^{A2} p \, dA + p_1 A_1 - p_2 A_2 \tag{5}$$

$$q_1 h_{v,1} + (1 - q_1) h_{l,(s),1} + \frac{u_1^2}{2} = q_2 h_{v,2} + (1 - q_2) h_{l,(s),2} + \frac{u_2^2}{2} \tag{6}$$

Where ρ_i, u_i, A_i, q_i and h_i denote the density, velocity, jet cross-section area, vapour phase mass fraction and specific enthalpy of vapor/liquid or vapor/solid CO_2 multiphase mixture at choked conditions (subscript 1) and fully expanded conditions (subscript 2). The pressure (*p*) at the free jet boundary is equal to the ambient pressure.

2.4 CFD modelling of external expansion

In order to verify the fully expanded conditions predicted by the analytical model, CFD simulations are performed. The key physical phenomena involved in the external expansion, including formation of shocks, phase change and generation of turbulence, are considered in CFD model. Homogeneous equilibrium flow is assumed as discussed in Section 2.1. The coupled governing equations are solved using ANSYS Fluent 14.0 with a pressure-based implicit scheme [19].

2.3.1 Computational domain

The computational domain is assumed to be axisymmetric. As can be seen in Figure 3, the large size (more than 100 nozzle diameters in axial direction) ensures the flow is atmospheric and subsonic at the outlets; high mesh density is implemented in the region close to the nozzle exit (labeled A) where the flow changes most rapidly.

(a) Sketch of the computational domain   (b) The mesh at the nozzle exit
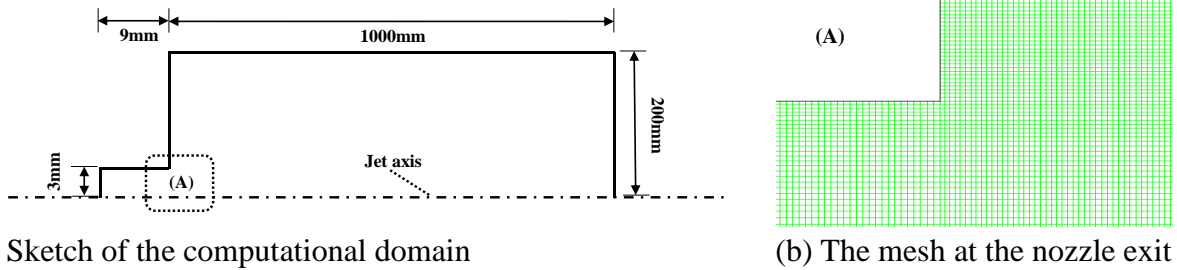
Figure 3: The computational domain and the mesh around the nozzle

In addition, after the first approximation of the flow field, mesh adaption based on normalised pressure gradients is utilised to assist in resolving the discontinuities. Figure 4 illustrates the refined mesh at the locations of the incident shock, the reflected shock and the Mach disk.
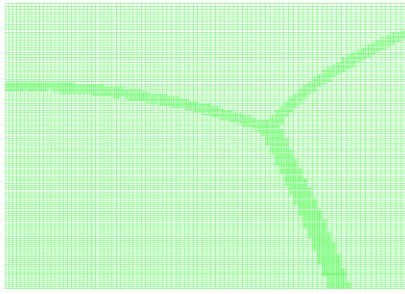

Figure 4: Demonstration of mesh adaption at the discontinuities

2.3.2 Turbulence modelling

During the external expansion, the turbulence generated at the jet boundary due to shear instabilities (Kelvin-Helmholtz) will develop and disturb the jet core until the jet is completely turbulent [10].

Since, only the average flow profile is necessary to obtain the fully expanded conditions and an axisymmetric computational domain is used, turbulence models based on the turbulent-viscosity hypothesis are selected. Compared to other models, such as Reynolds-stress models and Large Eddy Simulation (LES), they are much less computationally intensive by providing a convenient closure via the turbulent viscosity $(\mu_T(\boldsymbol{x},t))$, and therefore more practical towards high Reynolds number flow. The major assumption involved in these models is that the Reynolds-stress anisotropy $(a_{i,j})$ is dependent only on local process (i.e. local mean velocity gradients (Eq. 7)).

$$a_{i,j} = \overline{u_i'u_j'} - \frac{2}{3}k\delta_{ij} = -\frac{\mu_t}{\rho}\left(\frac{\partial \overline{U}_i}{\partial x_j} + \frac{\partial \overline{U}_i}{\partial x_i}\right) \tag{7}$$

The term on the right hand side can be written in terms of the mean rate-of-strain tensor $(a_{ij} = -2\frac{\mu_t}{\rho}\bar{S}_{ij})$, which is analogous to the Newtonian stress-rate-of-strain relation. However, turbulence could also be subjected to the straining history of the flow [20]. As a result,

5

turbulent-viscosity models are applied in the current study with the assumption that, the jet flow characteristics can be approximated by simple shear flow, where the production and dissipation of the turbulent kinetic energy is of the same order.

Among different turbulent-viscosity models, two-equation models are chosen over less complete ones such as the mixing-length model because of the difficulties of the specification of the mixing length relation for external flows. There are several well-established two-equation models, such as the k-ε model, the standard k-ω model and the k-ω Shear Stress Transport (SST) model. Compared to the k-ε model, the standard k-ω has the ability to correctly describe the turbulence in the boundary layers, especially in the case of adverse pressure gradients. In this study, predicting turbulence level within boundary layers (close to the nozzle wall) and therefore accurately modelling turbulence development has crucial impact on predicting the fully expanded conditions (especially for the momentums). However, the standard k-ω is very sensitive to the free stream specific dissipation rate (ω) [21], which makes it less applicable to supersonic flows. The SST formulation [22, 23], combining both features from the standard k-ω model and the k-ε model, has the capability of capturing turbulence in boundary layers and predicting free shear flows in high Reynolds number flow regime. The SST model transport equations are:

$$\frac{\partial(\rho k)}{\partial t} + \frac{\partial(\rho u_i k)}{\partial x_i} = P_k - \beta^* \rho k \omega + \frac{\partial}{\partial x_i}\left[(\mu + \sigma_k \mu_t)\frac{\partial k}{\partial x_i}\right] \tag{8}$$

$$\frac{\partial(\rho \omega)}{\partial t} + \frac{\partial(\rho u_i \omega)}{\partial x_i} = P_\omega - \beta \rho \omega^2 + 2\rho \sigma_{\omega,2}(1 - F_1)\frac{1}{\omega}\frac{\partial k}{\partial x_i}\frac{\partial \omega}{\partial x_i} \tag{9}$$

$$P_\omega = \alpha \rho S^2 + \frac{\partial}{\partial x_i}\left[(\mu + \sigma_\omega \mu_t)\frac{\partial \omega}{\partial x_i}\right] \tag{10}$$

Where P_k is the effective production rate of turbulent kinetic energy (k), P_ω is the production rate of specific dissipation rate (ω) and F_1 is the blending function through which model switching is enabled. Each invariant in the SST model ($\sigma_k, \sigma_\omega, \beta, \alpha$) is calculated by a combination of corresponding constants in the k-ε and the k-ω model in the form of Eq. 11.

$$\sigma_k = (1 - F_1)\sigma_{k,1} + F_1 \sigma_{k,2} \tag{11}$$

Where model constants with subscript 1 and 2 correspond to the k-ω and k-ε model respectively. Consequently, in close wall region, F_1 takes the value of 1 which corresponds to the standard k-ω formulation; away from wall region, F_1 takes the value of 0, which reduces the transport equation set to the k-ε model formulation.

In addition, modifications of the k transport equation (Eq. 8) are required to take the compressibility effect into account, because compressible flow field poses a short turbulent time scale. According to [24], the turbulent viscosity (μ_t) is related to the turbulent Mach number ($\mu_t = 0.09\rho\frac{k^2}{(1+M_t^2)\varepsilon}$), and a source term, $S_k = -\rho M_t^2 \varepsilon$, is introduced; M_t is the turbulent Mach number, which is defined as the ratio of $(2k)^{0.5}$ to local speed of sound (c).

3. General flow structure of expansion jets

In order to fully understand the external expansion process during the release, the general flow structure of an under-expanded jet is analysed.

Upon the flow exiting from the nozzle, expansion waves are formed, reducing the jet pressure smoothly until reflected by the free boundary to form a series of compression waves which eventually collapse to oblique shocks [16]. During this process, the jet expands below the ambient pressure. If the pressure mismatch at the exit is large, Mach reflections occurs when the incident oblique shocks meet the perimeter of the Mach disk (a strong normal shock). The flow normal to the Mach disk slows down whilst the pressure recovers above ambient pressure. The expansion-compression process repeats until the pressure stabilises at atmospheric pressure.

4. Results and discussions

4.1 Choked conditions
The isentropic expansion model discussed in section 2.2 has been applied to INERIS test 2, 3 and 4. The condensed phase volume fraction (φ_i) is also calculated. Table 1 summarises the predicted choked conditions.

Table 1: Reservoir conditions and predicted choked conditions

Chocked conditions:	T_1 (K)	p_1 (bar)	ρ_1 (kg/m^3)	u_1 (m/s)	q_1	φ_1
INERIS test 2	246.0	15.7	43.7	198.0	0.93	0.0028
INERIS test 3	260.7	24.7	72.8	188.4	0.89	0.0074
INERIS test 4	258.5	23.1	67.2	190.6	0.90	0.0062

For these tests, the large reservoir diameter to nozzle diameter ratio premises relatively steady stagnation conditions. Once the choked conditions have been obtained, it is then applied as inlet conditions in both the analytical and CFD external expansion models.

4.2 Analytical modelling results
Based on the choked conditions in section 4.1, external expansion analytical modelling is performed and the predicted flow variables at full expansion are presented in Table 2.

Table 2: Fully expanded conditions predicted by the analytical model

Fully expanded conditions:	T_2 (K)	p_2 (bar)	ρ_2 (kg/m3)	u_2 (m/s)	A_2 (m^2)	q_2	φ_2
INERIS test 2	194.0	1.0	3.07	367.5	0.00022	0.92	0.00016
INERIS test 3	194.0	1.0	3.10	361.0	0.00035	0.90	0.00019
INERIS test 4	194.0	1.0	3.09	363.3	0.00032	0.91	0.00018

4.3 CFD modelling results

Figure 5 contains the Mach number contour plots of the expansion jets, in which the flow field characteristics including the contact discontinuities, the incident/reflected oblique shocks and the Mach disks may be observed.

(a) INERIS test 2 (26.8bar, 264.3K)

(b) INERIS test 3 (42.0bar, 280.1K)

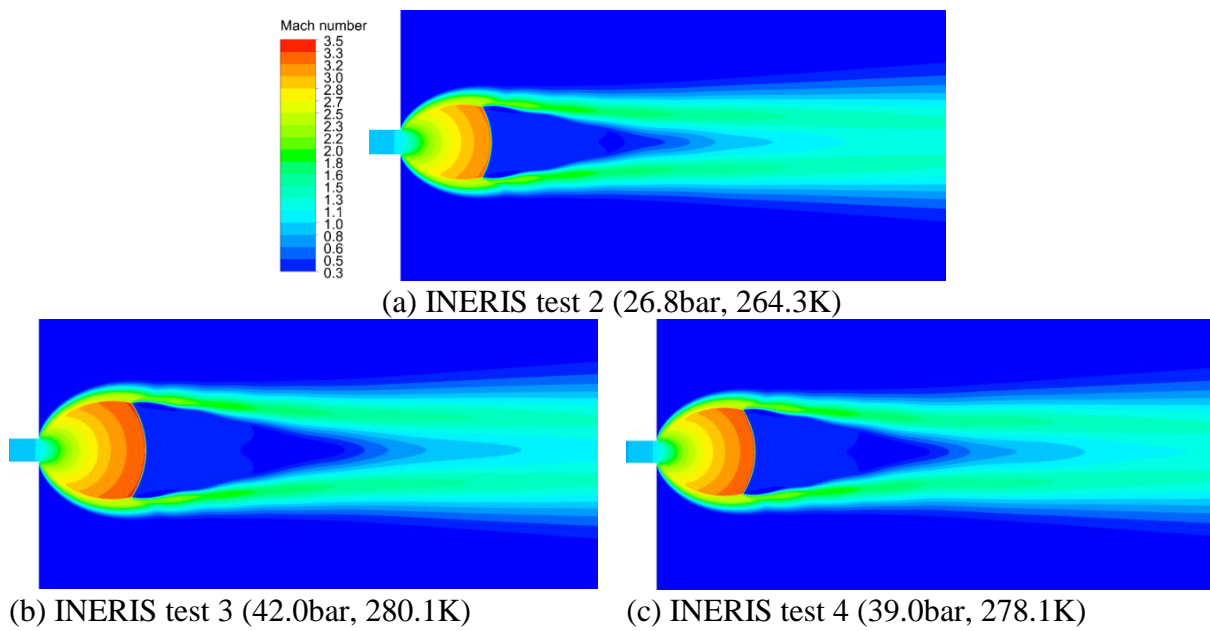(c) INERIS test 4 (39.0bar, 278.1K)

Figure 5: The Mach number contour plot

The flow variables along the jet centreline, including the temperature, the pressure and the condensed phase volume fraction are plotted in Figure 6. Following the jet structure discussion in Section 3, the discontinuity can be observed in all quantities at Mach disk. The jet is identified as fully expanded when the pressure stablises at ambient pressure, and since the both phases are at equilibrium, the temperature stays at 194K which is the saturated temperature of CO_2 at 1bar.
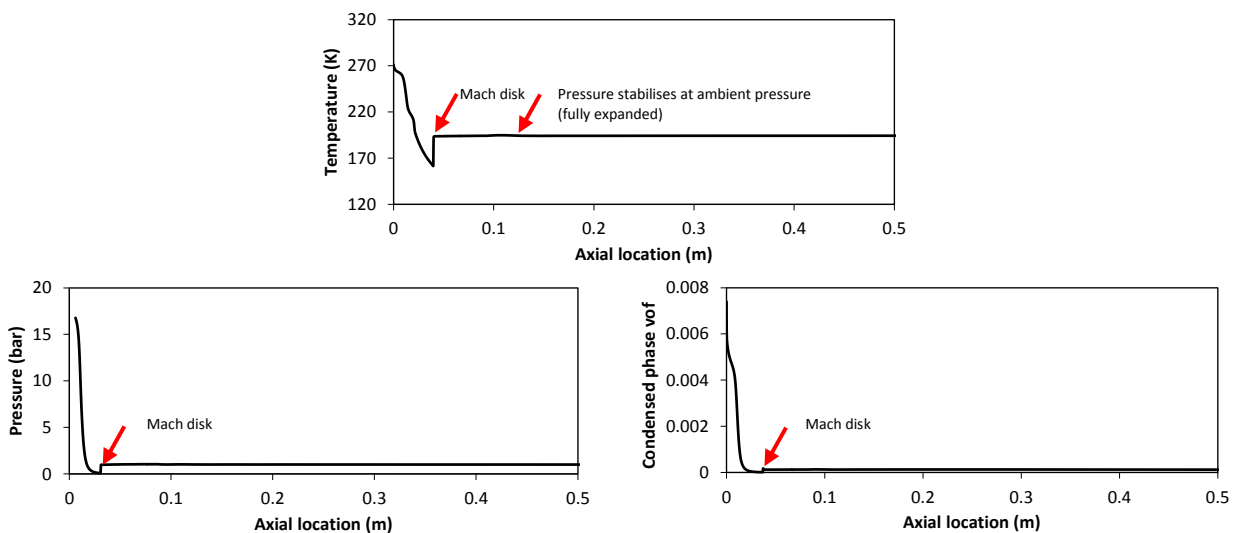

Figure 6: The flow profiles along the jet centreline (INERIS test 3)

4.4 Model comparisons and discussions

Figure 7, 10 and 11 show the predicted fully expanded conditions from both the analytical (dashed line) and the CFD modelling (solid line), including the velocity, the temperature and the density. Additionally, in order to make direct comparisons between the CFD and the analytical expansion model, the radial distributions of the flow variables at full expansion from the CFD modelling are averaged (dotted line). This is done by numerical integration

along the radius, whilst preserving the discharge mass flowrate, since entrainment is small before full expansion.

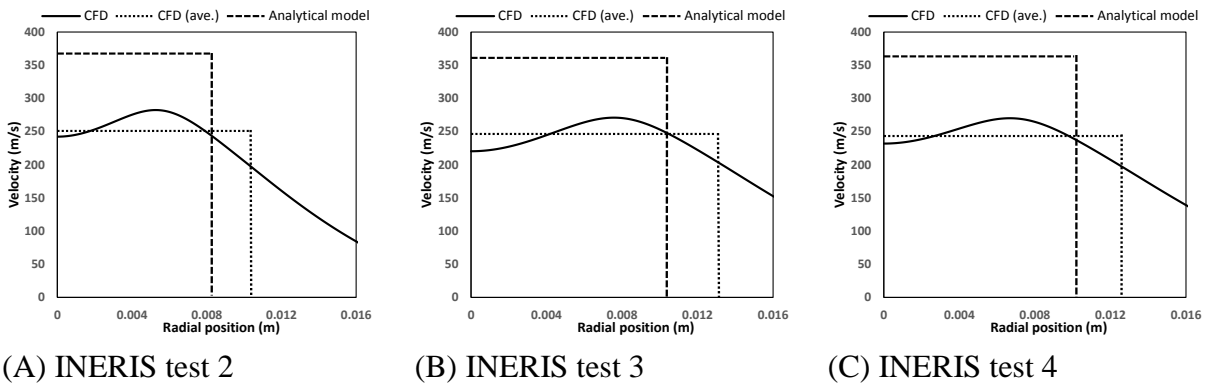(A) INERIS test 2   (B) INERIS test 3   (C) INERIS test 4

Figure 7: The velocity predictions at full expansion from the CFD and analytical model

Several general trends can be observed from the velocity plots. With the increase in the upstream reservoir pressure, the radius of the expanded jet increases while the corresponding velocity stays in the same vicinity (~350m/s by the analytical model and ~250m/s by the CFD model). From the model comparisons, the analytical model over-predicts the jet velocities at full expansion for all cases. The percentage difference between two models reaches up to approximately 40%. As for the expanded areas, the analytical model gives lower estimates (as shown in Figure 10, analytical model predicts smaller jet radius) because of the mass conservation at steady state.
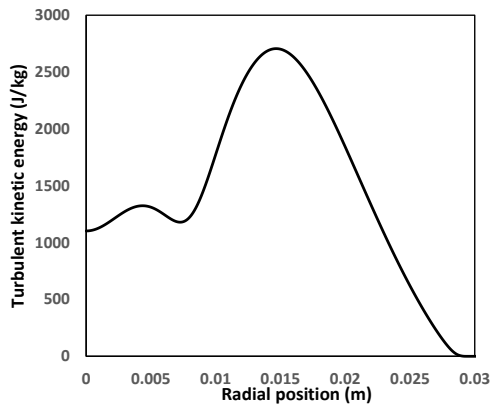

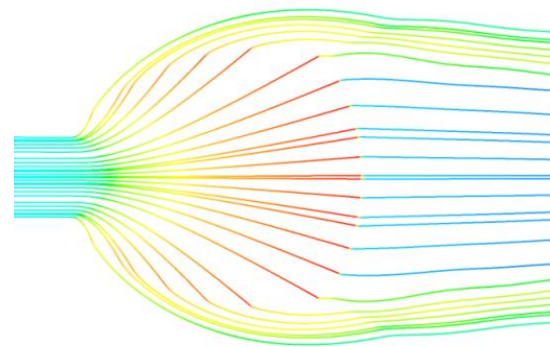Figure 8: The turbulent kinetic energy along the jet radius (INERIS test 3)

Figure 9: The streamlines of the flow field close to the nozzle

The overestimates were identified to arise from the no turbulence and quasi-one-dimensional flow assumption. During the repeated expansion-compression process after the Mach disk, turbulence in fact generates at the jet boundary due to shear and is transferred towards the jet core, promoting velocity fluctuations in the flow field. As can be seen in Figure 8, the peak turbulent kinetic energy occurs at jet free boundary (approximately 0.013m away from the jet centerline); and a considerable level of the turbulent kinetic energy which is directly related to the velocity fluctuations, indicates the development of turbulence throughout the jet cross-section area. Consequently, there is a loss in the momentum, hence the lower velocity predicted by the CFD model. From the streamline plot in Figure 9, by examining the

streamline directions, external expansion is highly multi-dimensional. The restricted dimension resulted from the analytical model assumption could also cause the deviation of the predicted fully expanded velocity from the CFD model.

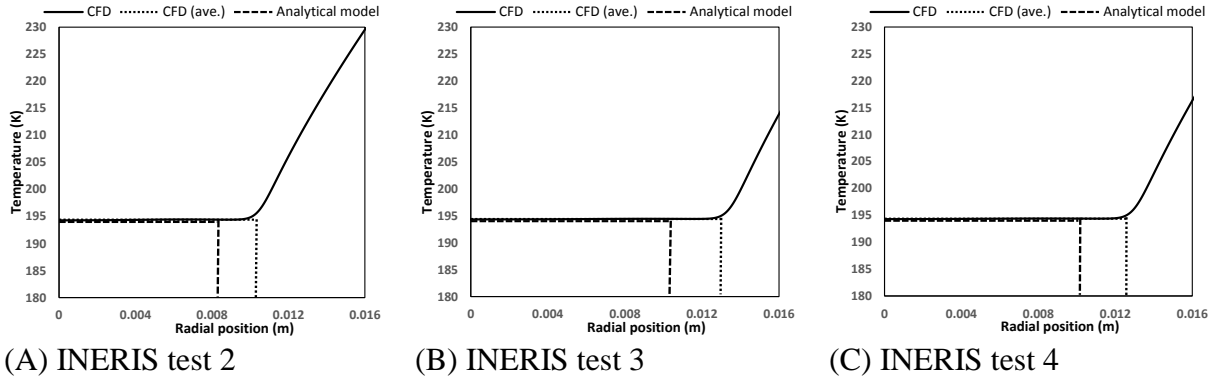(A) INERIS test 2　　(B) INERIS test 3　　(C) INERIS test 4

Figure 10: The temperature predictions at full expansion from the CFD and analytical model

Turning to thermodynamic predictions, for all cases, the temperature estimates (Figure 10) by both models agree. Given that Homogeneous Equilibrium is assumed for both models, after full expansion, the fluid will be at vapour-solid equilibrium at ambient pressure, the temperature predicted by the analytical model is expected to be in line with the CFD model.

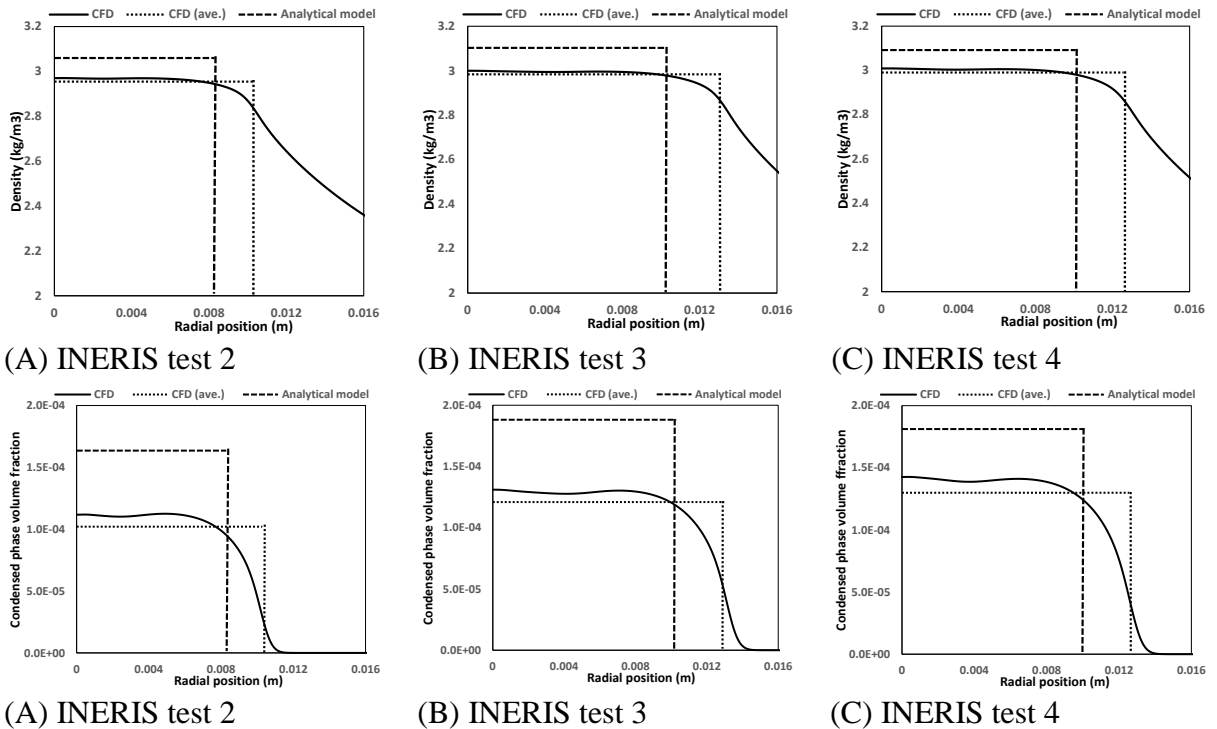(A) INERIS test 2　　(B) INERIS test 3　　(C) INERIS test 4

Figure 11: The density and the condensed phase volume fraction predictions at full expansion from the CFD and analytical model

Since the condensed phase (solid) exists at full expansion, the bulk density is determined by both the density of the individual phase and the condensed phase fraction. As may be observed in Figure 11, although the predictions of the condensed phase volume fraction at full expansion from both models differ by as much as 28%, those of the density are in close

agreement. This observation results from the fact that the amount of the condensed phase is small; according to the definition of the bulk density, a volume fraction of less than 0.0002 means a trifling contribution of the condensed phase to the bulk density. Therefore, a good analytical prediction of the fully expanded density may be restricted to the release scenarios where the resulted condensed phase is small.

5. Conclusions and future work

In this work, a conservation law based analytical model for predicting the flow following the expansion of multiphase jets was presented. For the purposes of verification the model was compared with the predictions form a turbulent multiphase CFD jet model.

It was found that, both the analytical model and CFD model predict a similar trend: while the velocity prediction at full expansion is not sensitive to larger stagnation pressure, the corresponding jet area increases. When the volume fraction of the condensed phase is small, the analytical model gives good temperature and density predictions in comparison with the CFD modelling results. In the case of the velocity (momentum) predictions, the analytical model however over-predicts up to 40% due to the assumptions of no generation of turbulence and quasi-one-dimensional flow.

Since the fully expanded conditions will be used as inputs in downstream dispersion modelling, in order to avoid overestimates of safety distance, hence increased pipeline routing difficulties, it is necessary to incorporate the turbulence effects, for example by using the empirical correlation for homogeneous turbulence [25]. Moreover, the actual impacts towards the subsequent dispersion, as a consequence of the over-predictions of the fully expanded jet momentum need to be analysed quantitatively. This will be done via CFD dispersion modelling using analytically predicted fully expanded conditions as inputs, from which the temperature and CO_2 concentration will be compared to the field data from the INERIS tests.

References

1. H. Pershad, K. Harland, A. Slewart, and S. Slater. CO_2 pipline Infrastructure : An analysis of global challenges and opportunities. Cambridge, 2010.
2. GlOBAL CCS INSTITUE. Strategic analysis of the global status of carbon capture and storage - Final report, 2009.
3. Iternational Energy Agency. Scenarios & Strategies to 2050. 2010.
4. M. M. J. Knoope, I. M. E. Raben, A. Ramírez, M. P. N. Spruijt, and A. P. C. Faaij. The influence of risk mitigation measures on the risks, costs and routing of CO_2 pipelines forthcoming. *Int. J. Greenh. Gas Control*, 29: pp. 104–124, 2014.
5. K. Patchigolla and J. E. Oakey. Design overview of high pressure dense phase CO_2 pipeline transport in flow mode. *Energy Procedia*, 37: pp. 3123–3130, 2013.
6. A. Oosterkamp and J. Ramsen. State-of-the-art overview of CO_2 pipeline transport with relevance to offshore pipelines. Haugesund, 2008.
7. R. K. Calay and A. E. Holdo. Modelling the dispersion of flashing jets using CFD. *J. Hazard. Mater.*, 154: pp. 1198–209, 2008.
8. G. Polanco, A. E. Holdø, and G. Munday. General review of flashing jet studies. *J. Hazard. Mater.*, 173: pp. 2–18, 2010.
9. X. Liu, A. Godbole, C. Lu, G. Michal, and P. Venton. Source strength and dispersion of CO_2 releases from high-pressure pipelines: CFD model using real gas equation of state. *Appl. Energy*, 126: pp. 56–68, 2014.

10. A. Hamzehloo and P. G. Aleiferis. Large eddy simulation of highly turbulent under-expanded hydrogen and methane jets for gaseous-fuelled internal combustion engines. *Int. J. Hydrogen Energy*, 39: pp. 21275–21296, 2014.
11. R. M. Woolley, M. Fairweather, C. J. Wareing, S. A. E. G. Falle, C. Proust, J. Hebrard, and D. Jamois. Experimental measurement and Reynolds-averaged Navier–Stokes modelling of the near-field structure of multi-phase CO_2 jet releases. *Int. J. Greenh. Gas Control*, 18: pp. 139–149, 2013.
12. T. Irie, T. Yasunobu, H. Kashimura, and T. Setoguchi. Characteristics of the mach disk in the underexpanded jet in which the back pressure continuously changes with time. *J. Therm. Sci.,*12: pp. 132–137, 2003.
13. A. Dauptain, B. Cuenot, and L. Y. M. Gicquel. Large Eddy Simulation of stable supersonic jet impinging on flat plate. *AIAA J.,* 48: pp. 2325–2338, 2010.
14. C. Proust, D. Jamois, and J. Hebrard. Experimental investigation of the dispersion of CO_2 in the atmosphere. 2013.
15. S. Martynov, S. Brown, and H. Mahgerefteh. An extended Peng-Robinson equation of state for carbon dioxide solid-vapor equilibrium. *Greenh. Gases Sci. Technol.,* 2: pp. 408–418, 2013.
16. J. Anderson. Modern compressible flow with historical perspective. *Internatio*. New York, 2004.
17. S. Martynov, S. Brown, H. Mahgerefteh, V. Sundara, S. Chen, and Y. Zhang. Modelling three-phase releases of carbon dioxide from high-pressure pipelines. *Process Saf. Environ. Prot.,* 92: pp. 36–46, 2014.
18. P. Bricard and L. Friedel. Two-phase jet dispersion. *J. Hazard. Mater.,* 59: pp. 287–310, 1998.
19. Fluent. ANSYS FLUENT User's Guide. 2011.
20. S. B. Pope. Turbulent Flows. Book, p. 771, 2000.
21. C. J. Roy and F. G. Blottner. Methodology for turbulence model validation: application to hypersonic flows. *J. Spacecr. Rockets*, 40: pp. 313–325, 2003.
22. F. R. Menter, M. Kuntz, and R. Langtry. Ten years of industrial experience with the SST turbulence model. *Turbul. Heat Mass Transf. 4*,4: pp. 625–632, 2003.
23. P. A. C. Rocha, H. H. B. Rocha, F. O. M. Carneiro, M. E. Vieira da Silva, and A. V. Bueno. *k-ω* SST (shear stress transport) turbulence model calibration: a case study on a small scale horizontal axis wind turbine. *Energy*, 65: pp. 412–418, 2014.
24. S. Sarkar, G. Erlebacher, M. Y. Hussaini, and H. O. Kreiss. The analysis and modelling of dilatational terms in compressible turbulence. *J. Fluid Mech.*, 227: pp. 473-493, 1991.
25. S. K. Lee, L. Djenidi, and R. A. Antonia. Empirical correlations for grid turbulence. *HEFAT2012*, pp. 215–221, 2012.